

An Efficient Quantum Circuit for Block Encoding a Pairing Hamiltonian

Diyi Liu¹, Weijie Du², Lin Lin^{3,4}, James P. Vary², and Chao Yang⁴

¹Department of Mathematics, University of Minnesota, Twin Cities, MN

²Department of Physics, Iowa State University of Minnesota, Ames, IA

³Department of Mathematics, University of California, Berkeley, CA

⁴Applied Mathematics and Computational Research Division, Lawrence Berkeley National Laboratory, Berkeley, CA

February 22, 2024

Abstract

We present an efficient quantum circuit for block encoding pairing Hamiltonians often studied in nuclear physics. Our block encoding scheme does not require mapping the creation and annihilation operators to the Pauli operators and representing the Hamiltonian as a linear combination of unitaries. Instead, we show how to encode the Hamiltonian directly using controlled swap operations. We analyze the gate complexity of the block encoding circuit and show that it scales polynomially with respect to the number of qubits required to represent a quantum state associated with the pairing Hamiltonian. We also show how the block encoding circuit can be combined with the quantum singular value transformation to construct an efficient quantum circuit for approximating the density of states of a pairing Hamiltonian. The techniques presented can be extended to encode more general second-quantized Hamiltonians.

1 Introduction

Block encoding is a recently developed technique for constructing Hamiltonian input model and enabling numerical linear algebra problems to be solved efficiently on a quantum computer [1, 2, 3]. By embedding a properly scaled matrix A into a larger unitary matrix U , one can perform the matrix vector multiplication Ax efficiently on a quantum computer by applying U to a quantum state prepared as $|x\rangle|0\rangle$ provided that U can be efficiently decomposed into simpler unitaries that form the building blocks (quantum gates) of a quantum circuit. When combined with quantum signal processing [2] and quantum eigenvalue/singular value transformation [4], which allow us to block encode a matrix function of A in terms of the block encoding of A , we can solve a variety of numerical linear algebra problems such as linear systems of equations, least squares problems and eigenvalue problems on a quantum computer [5, 6, 7].

A general block encoding scheme for sparse matrices was proposed in [4]. The construction of explicit block encoding quantum circuits has been shown in [1] for a few specific types of sparse matrices. Such constructions have also been developed for other types of sparse matrices in [8, 9, 10]. The explicit circuit construction for block encoding can be compressed for noisy intermediate-scale

quantum (NISQ) devices [11, 12, 13]. A hardware-efficient technique named Hamiltonian embedding has also been proposed for NISQ quantum computing [14]. Meanwhile, even if a matrix or an operator is dense, it can still be efficiently block encoded provided there exists special structure, for example, the matrix representation under another basis set is sparse [15, 16].

There is considerable interest in constructing efficient block encoding circuits for a second-quantized many-body Hamiltonian [17, 18]

$$\mathcal{H} = \sum_{i,j} h_{ij} c_i^\dagger c_j + \sum_{i<j, k<l} h_{ijkl} c_i^\dagger c_j^\dagger c_l c_k, \quad (1)$$

that arises in quantum chemistry and nuclear physics, where h_{ij} and h_{ijkl} denote the strength parameters that correspond to the one-body and two-body interactions of the electrons or nucleons. c_i^\dagger and c_i represent the fermionic creation and annihilation operators, with the index i labeling the single-fermion state. The Hamiltonian block-encoding scheme can be utilized in efficient quantum algorithms to perform dynamics simulations and structure calculations [19, 20, 21, 22].

A widely used technique to block encode \mathcal{H} is to transform the creation and annihilation operators to Pauli operators through the Jordan-Wigner [23] or Bravyi-Kitaev [24, 25] transformation, which enables one to rewrite (1) as a linear combination of Pauli unitaries. By combining a properly constructed preparation oracle circuit that encodes the coefficients for different terms in Eq. (1) and a selection oracle circuit that encodes the composition of Pauli operators, one can construct a quantum circuit for encoding a second quantized Hamiltonian.

In this paper, we present an alternative block encoding scheme for the pairing Hamiltonian that does not require mapping the creation and annihilation operators to Pauli operators. This scheme follows the procedure laid out in [1] to construct an explicit block encoding circuit of \mathcal{H} by treating it as a sparse matrix. In particular, we show how a unitary oracle circuit, which we denote by O_C later in this paper, that encodes the nonzero structure of \mathcal{H} can be constructed through the use of multi-qubit controlled swaps. The nonzero matrix elements of \mathcal{H} can be encoded by another unitary oracle circuit, which we denote by $O_{\mathcal{H}}$ later in the paper. This circuit can be implemented as a sequence of controlled rotations.

We demonstrate such a block encoding scheme and the corresponding quantum circuit by applying it to a simple pairing Hamiltonian for many-nucleon systems [26, 27]. The nuclear pairing interaction is a short-range attraction between nucleons. It contributes to the odd-even effect in the nuclear mass spectrum: that the total binding energy of an odd- A nucleus is less than the average of the total binding energies of the two neighboring nuclei with mass numbers $A \pm 1$ [27]. Besides the effects on nuclear binding energy, the nuclear pairing interaction also plays important roles on various other nuclear properties, such as the moment of inertia, the level-statistics of low-lying states, and the ground state distribution of nucleons in nuclei. The nuclear pairing interaction results from the pairwise correlations between nucleons, which is analogous to the correlated electron pairs in a metallic superconductor in condensed matter physics.

The pairing Hamiltonian [27] can be written as

$$\mathcal{H}_{\text{pair}} = \sum_{\alpha} \sum_{\beta} \sum_{m_{\alpha}>0} \sum_{m_{\beta}>0} G(\alpha, m_{\alpha}, \beta, m_{\beta}) c_{\alpha, m_{\alpha}}^\dagger c_{\alpha, -m_{\alpha}}^\dagger c_{\beta, -m_{\beta}} c_{\beta, m_{\beta}}, \quad (2)$$

where $G(\alpha, m_{\alpha}, \beta, m_{\beta})$ denotes the interaction coefficient. The creation operator $c_{\alpha, m_{\alpha}}^\dagger$ creates a state labelled as $|\alpha, m_{\alpha}\rangle$ with α denoting a set of quantum numbers (radial n_{α} , orbital angular momentum l_{α} and total angular momentum j_{α}) associated with a single-particle state and m_{α} being the absolute value of the projection of j_{α} . Similarly, $c_{\alpha, -m_{\alpha}}^\dagger$ creates the state labelled by $|\alpha, -m_{\alpha}\rangle$. We refer to the states $|\alpha, m_{\alpha}\rangle$ and $|\alpha, -m_{\alpha}\rangle$ as the paired single-particle states that

are created or annihilated jointly. The individual monomial $c_{\alpha, m_\alpha}^\dagger c_{\alpha, -m_\alpha}^\dagger c_{\beta, -m_\beta} c_{\beta, m_\beta}$ in $\mathcal{H}_{\text{pair}}$ first annihilates the paired single-particle states $|\beta, m_\beta\rangle$ and $|\beta, -m_\beta\rangle$ and then creates the paired states $|\alpha, m_\alpha\rangle$ and $|\alpha, -m_\alpha\rangle$ in a correlated manner.

For fermions, the creation and annihilation operators in (2) are subject to the anticommutation relations

$$\{c_{\alpha, \pm m_\alpha}^\dagger, c_{\beta, \pm m_\beta}\} = \delta_{\alpha, \beta} \delta_{m_\alpha, m_\beta}, \quad \{c_{\alpha, \pm m_\alpha}^\dagger, c_{\beta, \pm m_\beta}^\dagger\} = \{c_{\alpha, \pm m_\alpha}, c_{\beta, \pm m_\beta}\} = 0. \quad (3)$$

To simplify the notations, we define a mapping \mathcal{Q} between the quantum numbers $(n_\alpha, l_\alpha, j_\alpha, m_\alpha)$ associated with a single particle state and a unique integer so that

$$\mathcal{Q}(n_\alpha, l_\alpha, j_\alpha, m_\alpha) = 2p, \quad \mathcal{Q}(n_\alpha, l_\alpha, j_\alpha, -m_\alpha) = 2p + 1,$$

for a unique integer p . As a result, we can rewrite $c_{\alpha, m_\alpha}^\dagger$ simply as c_{2p}^\dagger and $c_{\alpha, -m_\alpha}$ as c_{2p+1}^\dagger . Similar simplification can be applied to the annihilation operators.

Since the single particle states indexed by $2p$ and $2p + 1$ are created or annihilated together, we can treat the creation or annihilation of these particle pairs as the creation or annihilation of a quasiparticle consisting of a correlated pair of fermions. We use the notation a_p^\dagger and a_p to denote the creation and annihilation of such a quasiparticle, respectively. With this notion, we express the pairing Hamiltonian simply as a (quasi) one-body operator

$$\mathcal{H}_{\text{pair}} = \sum_{p, q} h_{pq} a_p^\dagger a_q. \quad (4)$$

This paper is organized as follows. In section 2, we introduce the basic notations and conventions. We review the basic principles of block encoding and quantum signal processing in section 3. In section 4, we first review the general structure of a block encoding circuit for sparse matrices presented in earlier work [28]. We then show how the explicit circuit for the O_C oracle that encodes the nonzero structure of a (pseudo)one-body of Hamiltonian of the form (2) can be constructed by a sequence of multi-qubit swaps. We also show how the circuit for the $O_{\mathcal{H}}$ oracle that encodes the nonzero matrix elements of \mathcal{H} can be constructed as a sequence of controlled rotations. We give two examples to show how the circuit construction techniques presented in section 4 can be used to block encode a simple toy Hamiltonian and a pairing Hamiltonian in a Fock space defined by a limited number of single-particle basis states. We also show how such a block encoding circuit for the pairing Hamiltonian can be utilized to construct a quantum circuit that can be used to approximate the density of states of the Hamiltonian for all the systems describable in the chosen basis space. The latter requires us to use quantum signal processing/quantum eigenvalue transformation to construct a block encoding circuit for a matrix function of \mathcal{H} in terms of the block encoding circuit of \mathcal{H} . Additional comments are presented in section 6.

2 Notations and conventions

We adopt standard conventions used in the quantum computing literature [29] and use the Dirac $\langle \cdot |$ and $|\cdot\rangle$ notation to denote respectively row and column vectors. In particular $|0\rangle$ and $|1\rangle$ are used to represent the unit vectors $e_0 = [1 \ 0]^T$ and $e_1 = [0 \ 1]^T$, respectively. The tensor product of m $|0\rangle$'s is denoted by $|0^m\rangle$. We use $|x, y\rangle$ to represent the Kronecker product of $|x\rangle$ and $|y\rangle$, which is also sometimes written as $|x\rangle|y\rangle$ or $|xy\rangle$. The $N \times N$ identity matrix is denoted by I_N and we sometimes drop the subscript N when the dimension is clear in the context.

We map a binary representation of an integer $l \in \mathbb{N} : 0 \leq l \leq 2^n - 1$,

$$l = l_0 \cdot 2^0 + l_1 \cdot 2^1 + \dots + l_{n-1} \cdot 2^{n-1},$$

where $l_i \in \{0, 1\}$ for $i = 0, 1, 2 \dots n - 1$, to a quantum state $|l\rangle$ often written as $|l_0, \dots, l_{n-1}\rangle$. The superposition of these states can be encoded with n qubits where $|l_i\rangle$ is mapped to the i th qubit.

For a many-nucleon system, $|l_0, \dots, l_{n-1}\rangle$ can also be interpreted as an occupation representation of a many-body basis in which the value of l_i indicates the occupation of the i th single-particle state used to approximate a many-body state within a 2^n dimensional Hilbert space (Fock space).

We employ the letters H , X , Y , and Z to represent the Hadamard, Pauli- X , Pauli- Y , and Pauli- Z matrices, respectively. They are defined as

$$H = \frac{1}{\sqrt{2}} \begin{bmatrix} 1 & 1 \\ 1 & -1 \end{bmatrix}, \quad X = \begin{bmatrix} 0 & 1 \\ 1 & 0 \end{bmatrix}, \quad Y = \begin{bmatrix} 0 & -i \\ i & 0 \end{bmatrix}, \quad Z = \begin{bmatrix} 1 & 0 \\ 0 & -1 \end{bmatrix}. \quad (5)$$

These unitary matrices are used as single qubit gates in quantum computing.

We follow the standard convention for drawing quantum circuits with multiple parallel lines covered by several layers of rectangular boxes. Each line corresponds to either a single qubit or multiple qubits depending on how it is labelled and each box corresponds to a single qubit or multi-qubit gate depending on the number of qubit lines passing through it. We use the convention that the qubits in a circuit diagram are numbered increasingly from the top to the bottom as illustrated by the 3 qubit circuit U in Fig. 1. An integer $l = [l_{n-1} \dots l_1 l_0]$ input to a circuit is prepared as a quantum state $|l_0 \dots l_{n-1}\rangle$ with $|l_0\rangle$ mapped to the 0th qubit and $|l_{n-1}\rangle$ mapped to the $(n - 1)$ th qubit.

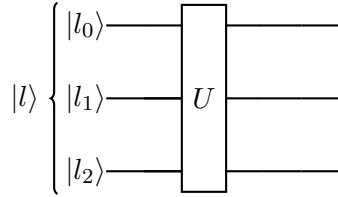


Figure 1: Illustration of the circuit convention. The circuit is prepared with Quantikz Package [30].

An important class of quantum gates are the controlled gates, i.e., one or more qubits act as a control for some operation. Graphically, the control operation is represented by a vertical line connecting the control qubit(s), marked by either a solid or open circle, to the so-called target gate, see e.g., the controlled NOT (CNOT) in Fig. 2. The target can also be multiple gates grouped in a subcircuit block used to perform certain operations. A solid circle indicates that the controlled operation is performed on the connected qubit, when the input to the controlling qubit is a $|1\rangle$ state. Similarly, an open circle indicates that the controlled operation is performed when the input to the controlling qubit is a $|0\rangle$ state.

$$\begin{array}{c} q_0 \text{---} \bullet \text{---} \\ | \\ q_1 \text{---} \oplus \text{---} \end{array} = \begin{bmatrix} 1 & 0 & 0 & 0 \\ 0 & 1 & 0 & 0 \\ 0 & 0 & 0 & 1 \\ 0 & 0 & 1 & 0 \end{bmatrix} \quad \begin{array}{c} q_0 \text{---} \circ \text{---} \\ | \\ q_1 \text{---} \oplus \text{---} \end{array} = \begin{bmatrix} 0 & 1 & 0 & 0 \\ 1 & 0 & 0 & 0 \\ 0 & 0 & 1 & 0 \\ 0 & 0 & 0 & 1 \end{bmatrix}$$

Figure 2: Illustration of Controlled-Not Gates.

Mathematically, the left and right controlled gates in Fig. 2 denote

$$E_1 \otimes X + (I - E_1) \otimes I, \quad \text{and} \quad E_0 \otimes X + (I - E_0) \otimes I, \quad (6)$$

respectively, where the orthogonal projection operators are

$$E_1 = e_1 e_1^T = |1\rangle \langle 1|, \quad E_0 = e_0 e_0^T = |0\rangle \langle 0|. \quad (7)$$

Note that the NOT (X) operation is applied to the input of qubit q_1 in the left circuit in Fig. 2 only if the input to qubit q_0 is $|0\rangle$. Likewise, the NOT operation is applied to the input of qubit q_1 in the right circuit in Fig. 2 if the input to qubit q_0 is $|1\rangle$. A similar expression can be used to denote multi-qubit controlled NOT gates.

3 Block encoding and quantum signal processing

Block encoding is a technique for embedding a properly scaled non-unitary matrix $A \in \mathbb{C}^{N \times N}$ into a unitary matrix U_A of the form

$$U_A = \begin{bmatrix} A & * \\ * & * \end{bmatrix}, \quad (8)$$

where $*$ denotes a matrix block yet to be determined. Applying U_A to a vector of the form

$$v = \begin{bmatrix} x \\ 0 \end{bmatrix} = |0\rangle |x\rangle, \quad (9)$$

yields

$$w = U_A v = \begin{bmatrix} Ax \\ * \end{bmatrix} = |0\rangle (A|x\rangle) + |1\rangle |*\rangle,$$

where $\|x\|_2 = 1$ and $*$ denotes a vector with unimportant information. If we measure the first qubit and obtain the $|0\rangle$ state, the second qubit register then contains $A|x\rangle$. The probability of such a successful measurement is $\|Ax\|^2$.

A more general definition of block encoding is as follows.

Definition 3.1 (Block encoding [1, 6]). Given an n -qubit matrix $A \in \mathbb{C}^{2^n \times 2^n}$, if we find $\alpha, \epsilon \in \mathbb{R}_+$, and an $(m+n)$ -qubit unitary matrix U_A so that

$$\|A - \alpha(|0^m\rangle \otimes I_{2^n}) U_A (|0^m\rangle \otimes I_{2^n})\| \leq \epsilon \quad (10)$$

then U_A is called an (α, m, ϵ) -block-encoding of A . In this paper, we only consider exact block encoding in which $\epsilon = 0$ and simply refer to U_A as an (α, m) -block-encoding.

Assuming U_A can be represented by an efficient quantum circuit, we can then apply A to a quantum state $|x\rangle$ on a quantum computer and generate $|Ax\rangle$ through the measurement of the ancilla qubits.

However, to solve the linear algebra problems involving A such as computing its lowest eigenvalue and corresponding eigenvector, we need to block encode a matrix function of A that is often approximated by a matrix polynomial. The quantum signal processing theory for scalar polynomials and its extension to matrix polynomials through the quantum singular value or eigenvalue transformation theory enables one to access the block encoding of a matrix polynomial of A on the basis of the block encoding of A .

For completeness, we present the quantum signal processing theory below, which is a slight variation of [4, Theorem 4].

Theorem 3.1 (Quantum signal processing). *Let*

$$U(t) = \begin{bmatrix} t & \sqrt{1-t^2} \\ \sqrt{1-t^2} & -t \end{bmatrix}, \quad (11)$$

where $|t| \leq 1$. There exists a set of phase angles $\Phi_d \equiv \{\phi_0, \dots, \phi_d\} \in \mathbb{R}^{d+1}$ so that

$$U_{\Phi_d}(t) \equiv (-i)^d e^{i\phi_0 Z} \prod_{j=1}^d [U(t) e^{i\phi_j Z}] = \begin{bmatrix} p(t) & -q(t)\sqrt{1-t^2} \\ q^*(t)\sqrt{1-t^2} & p^*(t) \end{bmatrix}, \quad (12)$$

if and only if $p(t)$ and $q(t)$ are complex valued polynomials in t and satisfy

1. $\deg(p) \leq d$, $\deg(q) \leq d-1$;
2. p has parity $d \bmod 2$, and q has parity $d-1 \bmod 2$;
3. $|p(t)|^2 + (1-t^2)|q(t)|^2 = 1$, $\forall t \in [-1, 1]$.

When $d = 0$, $\deg(q) \leq -1$ should be interpreted as $q = 0$.

Note that $U_{\Phi_d}(t)$ is a block encoding of the function p of a scalar t in Theorem 3.1. The theorem can be extended to a properly scaled matrix which is the theory behind quantum singular value transform (QSVT). When the block encoding of A , denoted by U_A , is Hermitian, QSVT reduces to quantum eigenvalue transformation (QET). It follows from QSVT that the block encoding of $p(A)$ for some polynomial $p(t)$ can be expressed in terms of the block encoding of A as illustrated in Fig. 3. In the circuit representation, ϕ_i is the same phase angle appearing in the Theorem 3.1. Each controlled-rotation gate CR_{ϕ_i} can be implemented as a single-qubit gate placed on the top ancilla qubit that performs $e^{-i\phi_i Z}$, preceded and followed by a multi-qubit CNOT gate [6]. We show the QSVT circuit for a specific example in the section 5.3. Although Theorem 3.1 only states the existence of such phase angles for quantum signal processing, these phase angles can be efficiently computed by solving a numerical optimization problem with a specific symmetric initial condition for phase angles [31, 32].

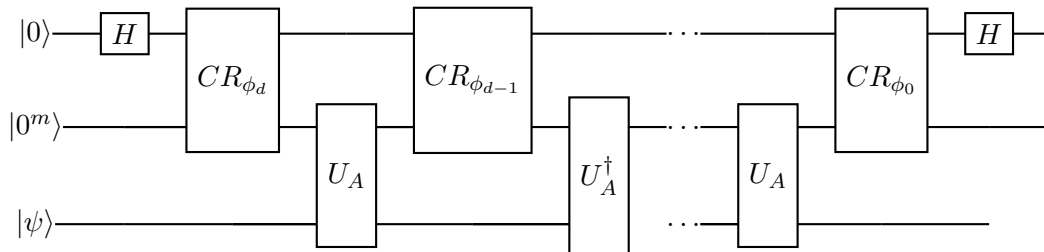


Figure 3: Illustration: the schematic circuit design of quantum singular value transformation (for an odd d ; for an even d the last U_A is replaced by U_A^\dagger). The additional Hadamard gate selects only the real part of the polynomial p .

4 Block encoding circuit

In this section, we describe how the second-quantized pairing Hamiltonian (4) can be block encoded and how an efficient quantum circuit can be constructed. When we consider a general pairing

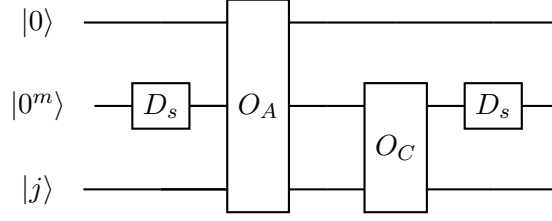


Figure 4: Illustration of the circuit for matrix block encoding.

Hamiltonian including self-energy term $c_p^\dagger c_p$, it is necessary to directly block encode the Hamiltonian written with creation and annihilation operator of fermions (2) (see section 5 for more details). To keep an concise notation for the creation and annihilation operator, we rewrite the Hamiltonian 4 and use an integer pair to label multiplication of a creation and an annihilation as shown in Eq. (4),

$$\mathcal{H}_{\text{pair}} = \sum_{p,q} h_{pq} a_p^\dagger a_q \equiv \sum_l v_l \mathcal{H}_l. \quad (13)$$

with the pair index $l \in \{(p, q) | 0 \leq p \leq n-1, 0 \leq q \leq n-1\}$. For each $l = (p, q)$, v_l is defined as h_{pq} in (13) and \mathcal{H}_l is defined as $a_p^\dagger a_q$. The relabeling does not lose any generality as a one-to-one mapping can be defined for the two sets notation for labeling fermionic system. We view $\mathcal{H}_{\text{pair}}$ as a sparse matrix. A general recipe for constructing a block encoding of an s -sparse matrix, which is defined to be a matrix that has at most s nonzero matrix elements in each column, is described by the following theorem (see [1, 4]).

Theorem 4.1. *Let $c(j, \ell)$ be a function that gives the row index of the ℓ th (among a list of s) non-zero matrix elements in the j th column of an s -sparse matrix $A \in \mathbb{C}^{N \times N}$ with $N = 2^n$, where $s = 2^m$. If there exists a unitary O_c such that*

$$O_c |\ell\rangle |j\rangle = |\ell\rangle |c(j, \ell)\rangle, \quad (14)$$

and a unitary O_A such that

$$O_A |0\rangle |\ell\rangle |j\rangle = \left(A_{c(j, \ell), j} |0\rangle + \sqrt{1 - |A_{c(j, \ell), j}|^2} |1\rangle \right) |\ell\rangle |j\rangle, \quad (15)$$

then

$$U_A = (I_2 \otimes D_s \otimes I_N) (I_2 \otimes O_c) O_A (I_2 \otimes D_s \otimes I_N), \quad (16)$$

block encodes A/s . Here D_s is called a diffusion operator and is defined as

$$D_s \equiv \underbrace{H \otimes H \otimes \dots \otimes H}_m, \quad (17)$$

The basic structure of the block encoding circuit is shown in Fig. 4.

Note that the input to the circuit consists of three set of qubits. The top qubit is used to encode nonzero matrix elements. The second set of qubits that take $|0^m\rangle$ as the input are used to encode the position of the nonzero elements. The bottom set of qubits that take $|j\rangle$ as the input are the qubits that encodes the column indices of the matrix to be block encoded.

The circuit consists of several blocks. The O_C block is used to encode the positions of the nonzero elements which is defined by the mapping $c(j, \ell)$ in Theorem 4.1. The O_A block is used to encode the nonzero matrix elements.

The structure of O_C depends on the mapping $c(j, \ell)$, which describes the sparsity structure of A . Ref. [1] showed how $c(j, \ell)$ is defined for tridiagonal Toeplitz matrices and sparse matrices whose sparsity structure can be described by a binary tree, as well as how the O_C circuit can be constructed efficiently for those type of matrices.

Once O_C is specified, we can construct O_A which encodes the numerical value of each non-zero matrix elements.

4.1 The O_C circuit

In this section, we describe how the O_C circuit can be constructed for the pairing Hamiltonian $\mathcal{H}_{\text{pair}}$ (13).

4.1.1 Define $c(j, \ell)$ by bit swap

The nonzero structure of the Hamiltonian is determined by the composition of the creation and annihilation operators in the second quantization representation of the Hamiltonian (2). The application of $a_p^\dagger a_q$ to the many-body basis $|j\rangle$ (a single Slater determinant) can potentially create a nonzero matrix element in the j th column of $\mathcal{H}_{\text{pair}}$ in the many-body basis. To understand such a non-zero structure, let us first consider the outcome of applying $a_p^\dagger a_q$ to a particular column $|j\rangle$ with a bit representation $|j_0 \cdots j_{n-1}\rangle$ where $j_k \in \{0, 1\}$. If $|j\rangle$ is a m particle state, then m of the n qubits are set to $|1\rangle$ while others are in $|0\rangle$. As a result, we can represent the state by an m -tuple $(f_0, f_1, \dots, f_{m-1})$ with f_0, f_1, \dots, f_{m-1} being the position of qubits in the $|1\rangle$ state. Alternatively, we can also represent $|j\rangle$ by

$$|j\rangle = a_{f_0}^\dagger a_{f_1}^\dagger \cdots a_{f_{m-1}}^\dagger |vac\rangle, \quad (18)$$

with $|vac\rangle$ denoting the vacuum state in which all the basis states are vacant.

If we use $|j\rangle_p$ to represent the p th bit in the binary representation of $|j\rangle$, it is easy to verify that for $\mathcal{H}_l = a_p^\dagger a_q$ defined in (13),

$$a_p^\dagger a_q |j\rangle = 0, \quad (19)$$

unless

$$\begin{cases} |j\rangle_q = |1\rangle \text{ and } |j\rangle_p = |0\rangle & \text{for } p \neq q, \\ |j\rangle_q = |1\rangle & \text{for } p = q. \end{cases} \quad (20)$$

In fact, if $|j\rangle$ satisfies (20), it is easy to show that

$$\begin{cases} [a_p^\dagger a_q |j\rangle]_p = |1\rangle, [a_p^\dagger a_q |j\rangle]_q = |0\rangle & \text{for } p \neq q, \\ [a_p^\dagger a_p |j\rangle]_p = |1\rangle & \text{for } p = q. \end{cases} \quad (21)$$

Therefore, the operator $a_p^\dagger a_q$ simply swaps the p th and q th bits in $|j\rangle$ (18) (the case with $p = q$ is trivial), creating a non-zero matrix element in the row whose index can be represented by the permuted bit string.

If $|j\rangle$ satisfies (20), the conditioned swap operation associated with \mathcal{H}_ℓ defines the $c(j, \ell)$ function in Theorem 4.1 as

$$c(j, \ell) = \begin{cases} \text{SWAP}(|j\rangle, p, q) & \text{if (20) holds,} \\ \text{invalid} & \text{otherwise,} \end{cases} \quad (22)$$

where $\text{SWAP}(|j\rangle, p, q)$ denotes the many-body state obtained from the binary representation of $|j\rangle$ by swapping the p -th qubit with the q -th qubit. When $c(j, \ell)$ is invalid, we can set it to any

arbitrary state, e.g., $|j\rangle$, and record the error information with an additional ancilla qubit (see discussions in section 4.1.3).

We should note that, in general, applying a one-body operator $a_p^\dagger a_q$ to $|j\rangle$ introduces a phase factor $(-1)^{j_{q+1}+j_{q+2}+\dots+j_{p-1}}$. Such a phase factor does not appear in encoding each \mathcal{H}_ℓ in $\mathcal{H}_{\text{pair}}$ (13) as a_p^\dagger and a_q are pseudo one-body operators that represent the creation and annihilation of the paired fermions in practice. In other words, the phase factor is always one as $j_{q+1} + j_{q+2} \dots + j_{p-1}$ is always an even integer in our example. The absence of the phase factors simplifies the O_C circuit construction.

4.1.2 The general structure of the O_C circuit

We note that the mapping between $|j\rangle$ and the valid $|c(j, \ell)\rangle$ involves a conditional swap operation, which is unitary. Therefore, we can use a controlled swap gate to implement O_C for \mathcal{H}_ℓ associated with a fixed ℓ . We discuss how such a controlled swap operation, which depends on both $|\ell\rangle$ and $|j\rangle$, can be implemented in the next section. The implementation requires two additional ancilla qubits to activate the control, and to discard invalid operations according to the possible error information.

To construct the O_C circuit for $\sum_{\ell=0}^{L-1} \mathcal{H}_\ell$, which defines the nonzero structure of \mathcal{H} defined in (13), we use a technique often referred to as a *select* oracle defined as

$$\text{select}(\mathcal{H}) = \sum_{\ell=0}^{L-1} |\ell\rangle \langle \ell| \otimes \mathcal{H}_\ell, \quad (23)$$

where ℓ corresponds to the pairwise indices (p, q) of the single-particle basis. We encode $|\ell\rangle$ with a set of ancilla qubits that is referred to as the *selection qubits*. The input to these qubits is the $|0\rangle^m$ state, where $m = \log L$. We use a diffusion operator (a set of Hadamard gates) to create a superposition of all possible ℓ 's, which enumerate all possible (p, q) pairs.

The selection oracle can be implemented as a product of controlled operations $S_{L-1} \dots S_1 \cdot S_0$, where

$$S_\ell = |\ell\rangle \langle \ell| \otimes \mathcal{H}_\ell + (I - |\ell\rangle \langle \ell|) \otimes I. \quad (24)$$

Here the projector $|\ell\rangle \langle \ell|$ serves as the control. When applied to $\frac{1}{2^{m/2}} \sum_{\ell=0}^{L-1} |\ell\rangle \otimes |j\rangle$, we obtain

$$\frac{1}{2^{m/2}} S_{L-1} \dots S_1 \cdot S_0 \sum_{\ell=0}^{L-1} |\ell\rangle \otimes |j\rangle = \frac{1}{2^{m/2}} \sum_{\ell=0}^{L-1} |\ell\rangle \otimes \mathcal{H}_\ell |j\rangle. \quad (25)$$

We combine the control (i.e., $|\ell\rangle \langle \ell|$) in (24) with the control used to implement (22). In particular, we need to include an ancilla qubit to invalidate operations in which the condition (20) does not hold, and some additional ancilla qubits to implement the controlled swap. For each ℓ , these controlled operations collectively define a unitary operator U_ℓ , that can be applied in sequence as shown in the circuit structure presented in Figure 5. Note that in this circuit, the validation qubit is set to $|1\rangle$ by the NOT (X) gate in advance. We assume the diffusion operator has already been applied to the $|0\rangle^m$ input to create a superposition of the $|\ell\rangle$ basis in the selection qubits.

4.1.3 The circuit for U_ℓ

We now discuss how the circuit for each U_ℓ can be constructed. As the swap operation is only performed when (20) is satisfied, such an operation should be carried out as a controlled swap.

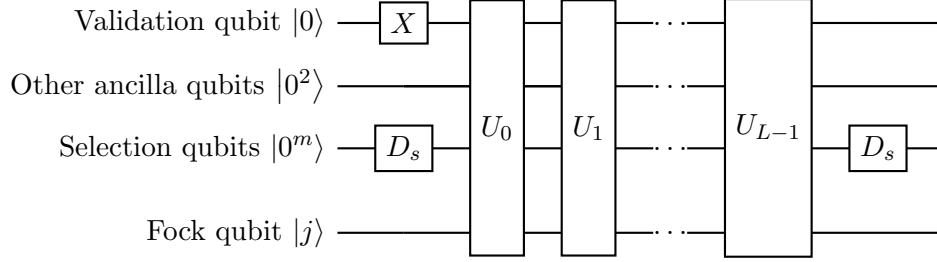


Figure 5: The basic structure of the O_C circuit. Qubits labeled by “Other ancilla qubits” consist of a controlling qubit and a rotation qubit as discussed in sections 4.1.3 and 4.2.

The control required to perform a specific swap operation for a particular pair of qubits is defined by both $|j\rangle$ and $|\ell\rangle$, i.e., the corresponding operator $a_p^\dagger a_q$. Since we can not place controls on the qubits to be swapped directly, we need an ancilla qubit to serve as a *controlling qubit* that activates the swap operation when that qubit is in the $|1\rangle$ state. In Figure 6, this controlling qubit is the second qubit from the top. The controlled swap is performed in the third layer from the end of the circuit.

The controlling qubit is initialized to the $|0\rangle$ state. It is turned to the $|1\rangle$ state when (20) holds for the input $|j\rangle$, which can be implemented as a set of controls placed on both $|\ell\rangle$ and $|j\rangle$ that are compatible. After a controlled swap operation is performed, we turn the validation qubit from $|1\rangle$

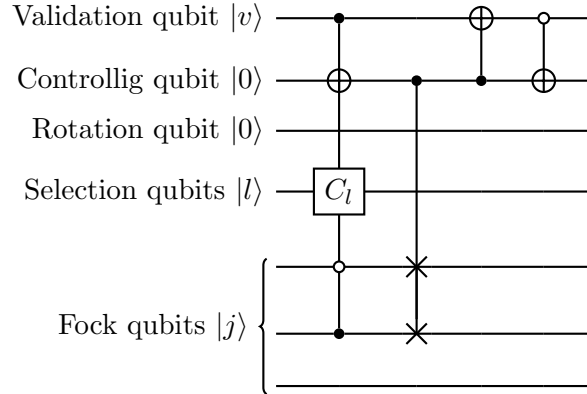


Figure 6: Illustration of U_l circuit with $\mathcal{H}_l = a_p^\dagger a_q$ and $p \neq q$.

to $|0\rangle$ by a CNOT gate (with a control placed on the controlling ancilla qubit) to indicate that a valid $\mathcal{H}_l |j\rangle$ has been performed. In addition, we use another CNOT gate (with a control placed on the validation qubit) to restore the controlling ancilla qubit to the $|0\rangle$ state as shown in the last layer of the circuit in Figure 6.

When $p = q$, no swap is needed when (20) holds. As a result, the corresponding U_l circuit, which is shown in Figure 7, can be simplified. The construction is similar to encode the self energy term $\sum_i c_i^\dagger c_i$ in the pairing Hamiltonian.

To illustrate the cumulative effect of applying $(I \otimes I \otimes D_s \otimes I)(X \otimes I \otimes I \otimes I)(U_{L-1} \cdots U_1 U_0)$ to the state $|0\rangle |0\rangle |0\rangle |j\rangle$, we consider a simple Hamiltonian of the form $\mathcal{H} = \mathcal{H}_0 + \mathcal{H}_1$, which requires a single selection qubit in the O_C circuit. We assume that both $(|0\rangle, |j\rangle)$ and $(|1\rangle, |j\rangle)$ satisfy (20). All intermediate quantum states produced from the application of each layer of the circuit shown

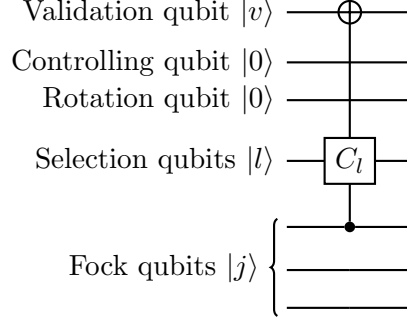


Figure 7: Illustration of U_l circuit with $\mathcal{H}_l = a_p^\dagger a_p$.

in Figure 5 (excluding the last D_s layer) to the input state are shown below.

$$\begin{aligned}
|0\rangle |0\rangle |0\rangle |j\rangle &\xrightarrow{D_s} \frac{1}{\sqrt{2}} |0\rangle |0\rangle |0\rangle |j\rangle + \frac{1}{\sqrt{2}} |0\rangle |0\rangle |1\rangle |j\rangle \\
&\xrightarrow{X} \frac{1}{\sqrt{2}} |1\rangle |0\rangle |0\rangle |j\rangle + \frac{1}{\sqrt{2}} |1\rangle |0\rangle |1\rangle |j\rangle \\
&\xrightarrow{U_0} \frac{1}{\sqrt{2}} |0\rangle |0\rangle |0\rangle |c(j, 0)\rangle + \frac{1}{\sqrt{2}} |1\rangle |0\rangle |1\rangle |j\rangle \\
&\xrightarrow{U_1} \frac{1}{\sqrt{2}} |0\rangle |0\rangle |0\rangle |c(j, 0)\rangle + \frac{1}{\sqrt{2}} |0\rangle |0\rangle |1\rangle |c(j, 1)\rangle
\end{aligned} \tag{26}$$

Taking the inner product of the last of line of (26) and $(I \otimes I \otimes D_s \otimes I) |0\rangle |0\rangle |0\rangle |i\rangle$ results in

$$\langle 0| \langle 0| \langle 0| \langle i| O_C |0\rangle |0\rangle |0\rangle |j\rangle = \frac{1}{2} [\delta(i, c(j, 0)) + \delta(i, c(j, 1))], \tag{27}$$

which correctly characterizes the nonzero structure of the j th column of \mathcal{H} . We note that (26) is independent of the sequence in which U_l 's acts.

If, for example, $(|1\rangle, |j\rangle)$ does not satisfy the condition (20), then it follows that

$$\begin{aligned}
|0\rangle |0\rangle |0\rangle |j\rangle &\xrightarrow{X, D_s} \frac{1}{\sqrt{2}} |1\rangle |0\rangle |0\rangle |j\rangle + \frac{1}{\sqrt{2}} |1\rangle |0\rangle |1\rangle |j\rangle \\
&\xrightarrow{U_0} \frac{1}{\sqrt{2}} |0\rangle |0\rangle |0\rangle |c(j, 0)\rangle + \frac{1}{\sqrt{2}} |1\rangle |0\rangle |1\rangle |j\rangle \\
&\xrightarrow{U_1} \frac{1}{\sqrt{2}} |0\rangle |0\rangle |0\rangle |c(j, 0)\rangle + \frac{1}{\sqrt{2}} |1\rangle |0\rangle |1\rangle |j\rangle.
\end{aligned} \tag{28}$$

In this case, the application of U_1 does not alter the second term on the right hand side of (28). Taking the inner product of the last line of (28) with $(I \otimes I \otimes D_s \otimes I) |0\rangle |0\rangle |0\rangle |i\rangle$, we obtain

$$\langle 0| \langle 0| \langle 0| \langle i| O_C |0\rangle |0\rangle |0\rangle |j\rangle = \frac{1}{2} \delta(i, c(j, 0)). \tag{29}$$

Compared to (27), we see that the invalid operation drops out in (29). The calculation showed how O_c can be constructed within a toy example. We summarize the result for more general application in the following theorem.

Theorem 4.2. Suppose there exist oracles U_i that works as

$$U_i : |v\rangle |l\rangle |j\rangle = \begin{cases} |0\rangle |l\rangle |c(j, l)\rangle & \text{if } i = l, v = 1 \text{ and satisfies (20),} \\ |v\rangle |l\rangle |j\rangle & \text{else,} \end{cases} \quad (30)$$

where $|v\rangle, |l\rangle, |j\rangle$ respectively indicates the state on validation qubit, selection qubit and Fock qubit, then O_C can be constructed as

$$O_C = (X \otimes I)U_0U_1 \dots U_{L-1} \quad (31)$$

and the O_C satisfies that

$$O_C : |0\rangle |l\rangle |j\rangle \rightarrow \begin{cases} |0\rangle |l\rangle |c(j, l)\rangle & \text{if satisfies (20),} \\ |1\rangle |l\rangle |j\rangle & \text{else.} \end{cases} \quad (32)$$

Proof. The proof follows from direct calculations. \square

4.2 The $O_{\mathcal{H}}$ circuit

The $O_{\mathcal{H}}$ circuit is used to encode nonzero matrix elements through controlled rotations. Since each nonzero element v_l is associated with the coefficient of a particular \mathcal{H}_ℓ term in (13), we construct a controlled rotation $O_{\mathcal{H}}^{(l)}$ for each coefficient as

$$O_{\mathcal{H}}^{(l)} |0\rangle |l\rangle |j\rangle = (v_l |0\rangle + \sqrt{1 - |v_l|^2} |1\rangle) |l\rangle |j\rangle, \quad (33)$$

when $l = (p, q)$ and j satisfy (20).

In the circuit implementation, we only need to place the control on the selection ancilla qubits $|l\rangle$. It is not necessary to place additional controls on the system qubit $|j\rangle$ because if l and j do not satisfy (20), the result of the controlled rotation will simply be discarded because the validation ancilla qubit will be in the $|1\rangle$ state after O_C is applied to the output of $O_{\mathcal{H}}$. Figure 8 gives an example of how $O_{\mathcal{H}}^{(l)}$ looks for some l represented by $|101\rangle$. The rotation $R_y(\theta_l)$ is applied to the “rotation qubit” with the rotation angle θ_l being $\arccos(v_l)$.

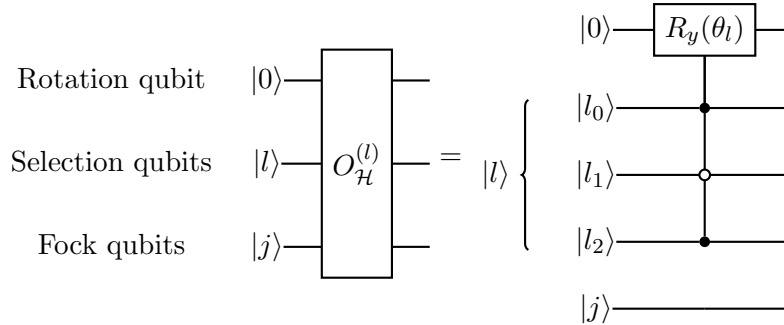


Figure 8: Illustration of $O_{\mathcal{H}}^{(l)}$ circuit for $l = |101\rangle$.

We note that the (p, q) pairs associated with different terms in (2) are mutually exclusive. Therefore, the $O_{\mathcal{H}}$ circuit can be implemented as a sequence of controlled rotations $O_{\mathcal{H}}^{(l)}$ ($l = 0, 1, 2, \dots, L - 1$) circuit components as shown in Figure 9, i.e.,

$$O_{\mathcal{H}} = O_{\mathcal{H}}^{(L-1)} O_{\mathcal{H}}^{(L-2)} \dots O_{\mathcal{H}}^{(1)} O_{\mathcal{H}}^{(0)}. \quad (34)$$

We remark that $O_{\mathcal{H}}$ is independent of the order of instruction of $O_{\mathcal{H}}^{(l)}$.

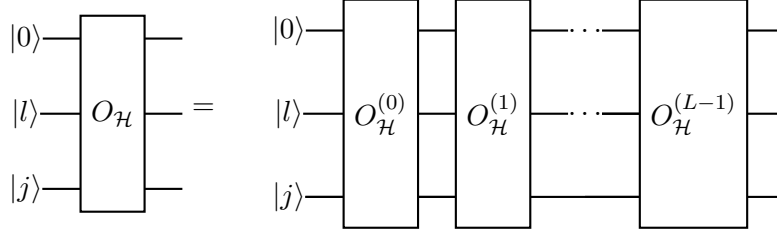


Figure 9: Illustration of $O_{\mathcal{H}}$ circuit.

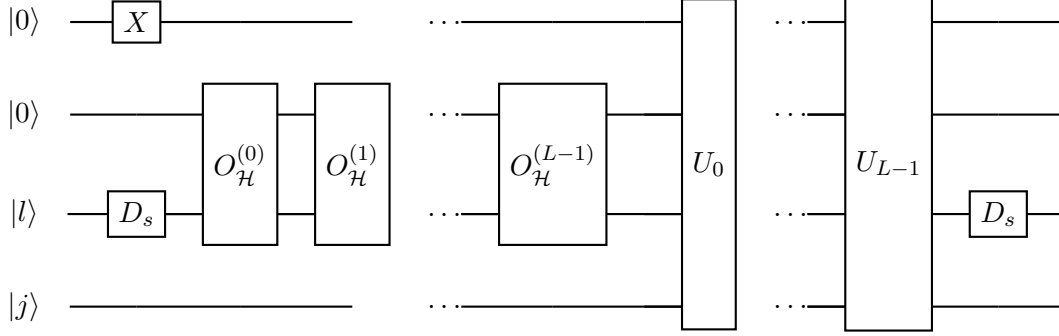


Figure 10: A schematic circuit design for the block encoding of $\mathcal{H}_{\text{pair}}$.

4.3 The complete circuit

The complete circuit for block encoding $\mathcal{H}_{\text{pair}}$ (13) is presented in Figure 10.

We now verify that such a circuit produces the desired output with the input to the circuit being $|0\rangle |0\rangle |0\rangle |0^m\rangle |j\rangle$. In particular, we have

$$\begin{aligned}
|0\rangle |0\rangle |0\rangle |0\rangle |0^m\rangle |j\rangle &\xrightarrow{X \otimes D_s} \frac{1}{\sqrt{s}} \sum_{l=0}^{L-1} |1\rangle |0\rangle |0\rangle |l\rangle |j\rangle \\
&\xrightarrow{O_{\mathcal{H}}} \frac{1}{\sqrt{s}} \sum_{l \in [s]} |1\rangle |0\rangle \left(v_l |0\rangle + \sqrt{1 - |v_l|^2} |1\rangle \right) |l\rangle |j\rangle \\
&\xrightarrow{O_C} \frac{1}{\sqrt{s}} \sum_{l \in [s]} |o(j, l)\rangle |0\rangle \left(v_l |0\rangle + \sqrt{1 - |v_l|^2} |1\rangle \right) |l\rangle |c(j, l)\rangle,
\end{aligned} \tag{35}$$

with $[s] = 0, 1, \dots, s-1$. We define $o(j, l)$ as

$$o(j, l) = \begin{cases} 0 & \text{if } l \text{ and } j \text{ satisfy (20),} \\ 1 & \text{otherwise.} \end{cases} \tag{36}$$

By taking the inner product of the output of (35) with $(I \otimes I \otimes I \otimes D_s \otimes I) |0\rangle |0\rangle |0\rangle |0^m\rangle |i\rangle$, we obtain

$$\langle 0 | \langle 0 | \langle 0 | \langle 0^m | \langle i | U_{\mathcal{H}} |0\rangle |0\rangle |0\rangle |0^m\rangle |j\rangle = \frac{1}{s} v_l \delta(i, c(j, l)), \tag{37}$$

when $o(j, l) = 0$. Otherwise, this matrix element is 0 due to the vanishing inner product between $|0\rangle$ and $|1\rangle$ of the validation qubit.

4.4 Gate complexity

The complete block encoding circuit shown in Figure 10 contains $L U_\ell$ -blocks, where L is the number of creation and annihilation pairs in (4). Each one of these blocks consists of at most one $\log(L) + 3$ qubit CNOT gate and one single qubit controlled swap gate as well as two standard CNOT gates as we have shown in section 4.1.3. The multi-qubit control gate can be decomposed into $2 \log(L) + 3$ three-qubit Toffoli gates [33]. Each three-qubit Toffoli gate can in turn be decomposed into seven T gates and six CNOT gates [34]. The control swap in each U_ℓ block can be implemented as two standard CNOTs. Therefore, in total, each U_ℓ block requires $12 \log(L) + 22$ CNOT gates and $14 \log(L) + 21$ T gates. Assume each controlled rotation gate can be directly implemented and each such gate is counted as one two-qubit gate, then in the complete block encoding circuit, there are L two-qubit gates for controlled rotation. Adding up all these gate counts, we estimate the circuit requires $12L \log(L) + 23L$ two-qubit gates and $14L \log(L) + 21L$ T gates. Because L is generally a polynomial of $n = \log N$, the overall gate complexity of the circuit is $\mathcal{O}(\text{poly}(n) \log(n))$. We should note that our estimation here assumes the quantum computer we work with has all-to-all connectivity and can perform an arbitrary single-qubit rotation for any angle. In practice, these assumption may not hold for the current generation of noisy intermediate-scale quantum (NISQ) devices. A more detailed analysis of the gate count for a particular quantum computer is beyond the scope of this paper.

5 Numerical examples

In this section, we give two examples of explicit circuit design for second-quantized Hamiltonians. The first examples involves a toy Hamiltonian with 4 (pseudo) one-body terms. The second example consists of a Hamiltonian constructed in a Fock space defined by a limited number of single-particle states.

5.1 O_C for a simple example

In this section, we will examine how a block encoding circuit can be constructed for the following simple model Hamiltonian

$$\mathcal{H} = \underbrace{a_0^\dagger a_0}_{\mathcal{H}_0} + \underbrace{a_0^\dagger a_1}_{\mathcal{H}_1} + \underbrace{a_1^\dagger a_0}_{\mathcal{H}_2} + \underbrace{a_1^\dagger a_1}_{\mathcal{H}_3}, \quad (38)$$

using the techniques discussed above. Since the coefficient for each \mathcal{H}_l in (38) is 1, we only need to examine the O_C circuit as $O_{\mathcal{H}}$ is simply an identity. Each creation and annihilation operator is for a pair of nucleons and due to the form of the Hamiltonian, only the states with occupied nucleon pairs will be nonzero. It suffice to only encode the Hamiltonian for the states where nucleons appear in pairs as all other states will vanish under the Hamiltonian. Because there are four terms in the Hamiltonian, we use $l = 0, 1, 2, 3$ to index each term, and map the binary representation of $l = l_0 + 2l_1$ with $l_0, l_1 \in \{0, 1\}$ to the ancilla qubits labelled by $|l_0\rangle$ and $|l_1\rangle$ in Figure 11. Furthermore, since there are only two particles involved in the Hamiltonian, we use two system qubits labeled as $|j_0\rangle$ and $|j_1\rangle$ with $j_0, j_1 \in \{0, 1\}$ to represent a computational basis in the 4-dimensional Fock space associated with the Hamiltonian \mathcal{H} defined in (38). Figure 11 and Figure 12 illustrate the explicit construction of each U block defined in Theorem 4.2 for the Hamiltonian (38).

To illustrate the effect of each layer of the circuit, we show the input to the quantum circuit, the intermediate state produced by each layer of the O_C circuit, and the output state in Figure 13. In step 1, a multi-qubit control is used to ensure the controlling qubit is turned into $|1\rangle$ only when the three conditions listed in Theorem 4.2 are satisfied. If any one of them is violated, then the first

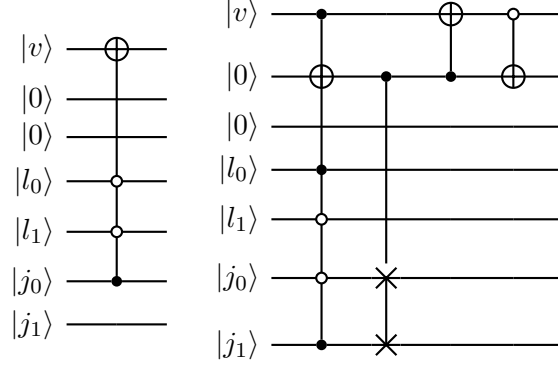


Figure 11: The left panel shows U_0 circuit with $\mathcal{H}_0 = a_0^\dagger a_0$ and the right panel shows U_1 circuit with $\mathcal{H}_1 = a_0^\dagger a_1$.

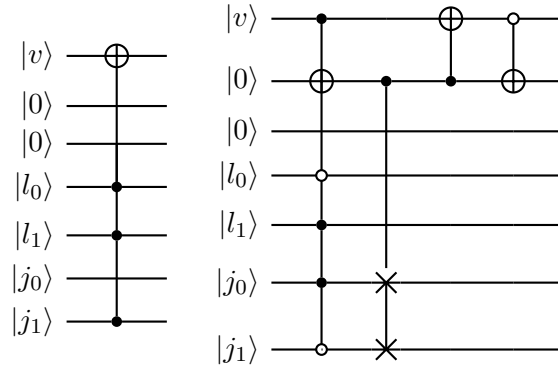


Figure 12: The left panel shows U_3 circuit with $\mathcal{H}_3 = a_1^\dagger a_1$ and the right panel shows U_2 circuit with $\mathcal{H}_2 = a_1^\dagger a_0$.

layer of the circuit does nothing to the input state. In step 2, a control swap operation is applied under condition of the controlling qubit being $|1\rangle$. This indicates the action of $\mathcal{H}_1 = a_0^\dagger a_1$ on the Fock state when all the three conditions are satisfied. In step 3, a CNOT is applied to the validation qubit, in order to record that the output is valid and should be saved for final computation. In step 4, another CNOT is applied to uncompute the controlling qubit.

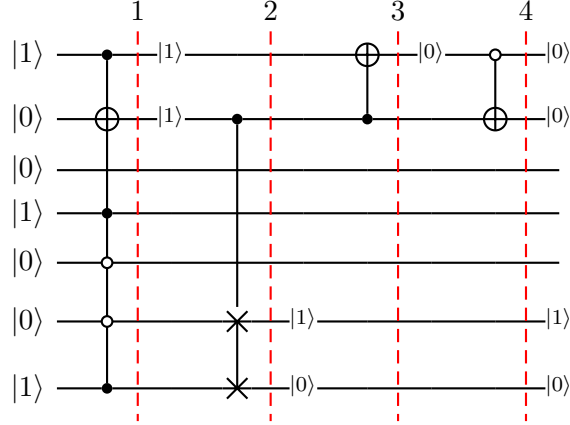


Figure 13: Illustration of the action of U_1 on the state $|1\rangle |l\rangle |j\rangle$ with $l = 1$ and $|j\rangle = a_1^\dagger |vac\rangle$

5.2 The three-nucleon system with the pairing Hamiltonian

In this subsection, we present the circuit to block encode a simple pairing Hamiltonian $\mathcal{H}_{\text{pair}}$ (2) and possible applications based on our block encoding scheme. Instead of block encoding the Hamiltonian with one-body pseudo-particle creation and annihilation operators, we illustrate how to extend the circuit construction according to (2) with same idea discussed above. In particular, we elect to demonstrate our scheme with the three-nucleon problem in Ref. [35]. For this model problem, we choose a set of six single-particle bases shown in Table 1. Each single particle basis is labeled by a set of quantum numbers $\{n_\alpha, l_\alpha, j_\alpha, m_{j_\alpha}\}$, where $m_{j_\alpha} = \pm m_\alpha$ as we explained in section 1. We omit the spin, which is taken to be $1/2$ for the nucleons. In our demonstration, we do not distinguish between protons and neutrons; hence we also omit the isospin degree of freedom in our basis. With the mapping defined in Table 1, we can label each single particle basis by an integer listed in the first column of Table 1 and rewrite the pairing Hamiltonian as

$$\begin{aligned}
 \mathcal{H}_{\text{pair}} = & c_0^\dagger c_1^\dagger c_1 c_0 + c_0^\dagger c_1^\dagger c_3 c_2 + c_0^\dagger c_1^\dagger c_5 c_4 \\
 & + c_2^\dagger c_3^\dagger c_1 c_0 + c_2^\dagger c_3^\dagger c_3 c_2 + c_2^\dagger c_3^\dagger c_5 c_4 \\
 & + c_4^\dagger c_5^\dagger c_1 c_0 + c_4^\dagger c_5^\dagger c_3 c_2 + c_4^\dagger c_5^\dagger c_5 c_4.
 \end{aligned} \tag{39}$$

5.2.1 Construction of O_C oracle

As the coefficient for each term in the Hamiltonian given by (39) is 1, it is sufficient to consider only the O_C circuit for the block encoding of $\mathcal{H}_{\text{pair}}$. Instead of encoding a nucleon pair with a qubit, we construct the block encoding with the direct encoding scheme of the single-particle states. In the Hamiltonian, there are in total 9 pairing terms where each term can be labeled by a pair of indices (l_1, l_2) that specify the pairing term,

Table 1: The restricted single-particle basis set for a single-species three-nucleon system. See text for details.

single-particle basis (qubit) index	quantum numbers			
	n	l	$2j$	$2m_j$
0	0	0	1	-1
1	0	0	1	+1
2	1	0	1	-1
3	1	0	1	+1
4	2	0	1	-1
5	2	0	1	+1

$$c_{2l_1}^\dagger c_{2l_1+1}^\dagger c_{2l_2+1} c_{2l_2} \quad (40)$$

where $l_1, l_2 \in \{0, 1, 2\}$.

The O_C circuit can be constructed via a sequence of U_{l_1, l_2} blocks. We illustrate the explicit construction in the Fig. 14. We still follow our circuit design in previous section but explicitly encode the state of each nucleon clearly, i.e. $|j_0\rangle, |j_1\rangle, |j_2\rangle, |j_3\rangle, |j_4\rangle, |j_5\rangle$ each represents nucleon is occupied or not. The condition on l_1 and l_2 is transformed into the multi-control of binary representation of l_1 and l_2 . The condition of 20 is equivalent to the the control of $|j_0, j_1\rangle = |00\rangle$ and $|j_2, j_3\rangle = |11\rangle$. The swap operation in the formalism is the swap between the state $|j_0, j_1\rangle$ and $|j_2, j_3\rangle$ and it could be implemented as four CNOT gate in practice.

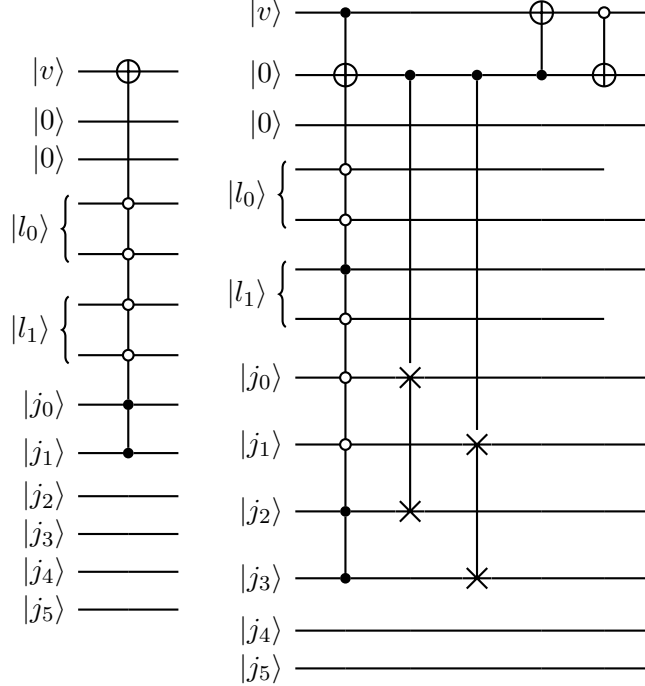


Figure 14: The left panel shows circuit of $U_{0,0}$ corresponds to $c_0^\dagger c_1^\dagger c_1 c_0$ and the right panel shows $U_{0,1}$ circuit with $c_0^\dagger c_1^\dagger c_3 c_2$.

5.2.2 Verification of block encoding

In this subsection, we validate the block encoding circuit by evaluating the output of the circuit when a particular computational basis is chosen as the input. For this three-nucleon system in the restricted single-particle basis set (Table 1), we have $\binom{6}{3} = 20$ three-nucleon states in total yielding a 20×20 Hamiltonian matrix. The Hamiltonian can be block diagonalized and partitioned according to the M_J value of a many-body state. In particular, there are 1) 9 states with $M_J = -\frac{1}{2}$; 2) 9 states with $M_J = +\frac{1}{2}$; 3) 1 state with $M_J = -\frac{3}{2}$; and 4) 1 state with $M_J = +\frac{3}{2}$. We sort these three-nucleon states in Table 2. The states associated with a distinct M_J value form an invariant subspace of $\mathcal{H}_{\text{pair}}$. For this problem, we can evaluate the matrix elements of the pairing Hamiltonian within each diagonal block associated with a distinct M_J value analytically. The many-nucleon basis states that span each invariant subspace associated with a distinct M_J value are shown in Table 2. The diagonal block associated with $M_J = +\frac{1}{2}$, which corresponds to the invariant subspace spanned by the states

$$(0, 1, 3), (0, 1, 5), (0, 3, 5), (1, 2, 3), (1, 2, 5), (1, 3, 4), (1, 4, 5), (2, 3, 5), (3, 4, 5),$$

for example, has the form

$$\mathcal{H}_{\text{pair}}(M_J = +\frac{1}{2}) = \begin{pmatrix} 1 & 0 & 0 & 0 & 0 & 0 & 0 & 0 & 0 & 1 \\ 0 & 1 & 0 & 0 & 0 & 0 & 0 & 0 & 1 & 0 \\ 0 & 0 & 0 & 0 & 0 & 0 & 0 & 0 & 0 & 0 \\ 0 & 0 & 0 & 1 & 0 & 0 & 1 & 0 & 0 & 0 \\ 0 & 0 & 0 & 0 & 0 & 0 & 0 & 0 & 0 & 0 \\ 0 & 0 & 0 & 0 & 0 & 0 & 0 & 0 & 0 & 0 \\ 0 & 0 & 0 & 1 & 0 & 0 & 1 & 0 & 0 & 0 \\ 0 & 1 & 0 & 0 & 0 & 0 & 0 & 0 & 1 & 0 \\ 1 & 0 & 0 & 0 & 0 & 0 & 0 & 0 & 0 & 1 \end{pmatrix}. \quad (41)$$

Table 2: The three-nucleon states sorted according to M_J . Only the indices of the occupied single-particle states are recorded, where the quantum numbers of each single-particle state are shown in Table 1. For example, the three-nucleon state $(0, 1, 3)$ is equivalent to $|110100\rangle$ in notations.

M_J	three-nucleon state								
$+3/2$	(1, 3, 5)	-	-	-	-	-	-	-	-
$+1/2$	(0, 1, 3)	(0, 1, 5)	(0, 3, 5)	(1, 2, 3)	(1, 2, 5)	(1, 3, 4)	(1, 4, 5)	(2, 3, 5)	(3, 4, 5)
$-1/2$	(0, 1, 2)	(0, 1, 4)	(0, 2, 3)	(0, 2, 5)	(0, 3, 4)	(0, 4, 5)	(1, 2, 4)	(2, 3, 4)	(2, 4, 5)
$-3/2$	(0, 2, 4)	-	-	-	-	-	-	-	-

We now verify the correctness of the block encoding circuit by examining the output of the circuit when the input of the circuit is initialized as $|110100\rangle$ which corresponds to the state $(0, 1, 3)$. This state is mapped to the first column $\mathcal{H}_{\text{pair}}(M_J = +\frac{1}{2})$ defined in (41).

$$\begin{aligned}
|0\rangle |0^2\rangle |0^2\rangle |110100\rangle &\xrightarrow{X \otimes D_s} \frac{1}{\sqrt{16}} \sum_{l_1=0}^3 \sum_{l_2=0}^3 |1\rangle |l_1\rangle |l_2\rangle |110100\rangle \\
&\xrightarrow{O_{\mathcal{H}=I}} \frac{1}{\sqrt{16}} \sum_{l_1=0}^3 \sum_{l_2=0}^3 |1\rangle |l_1\rangle |l_2\rangle |110100\rangle \\
&\xrightarrow{U_{0,0}} \frac{1}{\sqrt{16}} |0\rangle |0\rangle |0\rangle |110100\rangle + \frac{1}{\sqrt{16}} \sum_{(l_1, l_2) \neq (0,0)} |1\rangle |l_1\rangle |l_2\rangle |110100\rangle, \\
&\xrightarrow{U_{0,1}} \frac{1}{\sqrt{16}} |0\rangle |0\rangle |0\rangle |110100\rangle + \frac{1}{\sqrt{16}} |1\rangle |0\rangle |1\rangle |110100\rangle, \\
&+ \frac{1}{\sqrt{16}} \sum_{(l_1, l_2) \neq (0,0), (0,1)} |1\rangle |l_1\rangle |l_2\rangle |110100\rangle \\
&\dots\dots \\
&\xrightarrow{U_{2,2}} \frac{1}{\sqrt{16}} |0\rangle |0\rangle |0\rangle |110100\rangle + \frac{1}{\sqrt{16}} |0\rangle |0\rangle |2\rangle |000111\rangle + \frac{\sqrt{14}}{\sqrt{16}} |1\rangle |\Psi\rangle |110100\rangle
\end{aligned} \tag{42}$$

where $\Psi = \sum_{(l_1, l_2) \neq (0,0), (0,1)} |l_1\rangle |l_2\rangle$. Taking the inner product of the last line of (42) with $(I \otimes D_s \otimes I) |\phi\rangle$ results in 0 unless $|\phi\rangle = |110100\rangle$ or $|000111\rangle$. These two states correspond to the first and last rows of the matrix given in (41). For these two states, the inner product yields $1/16$. Similar verification can be made for other input states that correspond exactly to other columns of the matrix (41), which ultimately shows that the circuit constructed above indeed produces a (16,5)-block encoding of $\mathcal{H}_{\text{pair}}(M_J = +\frac{1}{2})$.

5.3 The density of states via the block-encoded pairing Hamiltonian

In the section, we utilize the block encoding circuit of the pairing Hamiltonian to construct an explicit circuit for approximating the density of states (DOS) of the scaled pairing Hamiltonian $\mathcal{H}'_{\text{pair}}$ for all the many-body systems allowed by the restricted basis set. This example serves to demonstrate an application of the block encoding. The DOS of the pairing Hamiltonian $\mathcal{H}_{\text{pair}}$ within the Hilbert space defined by all allowed fermion occupancies of the $n = 6$ single-particle states described in section 5.2 can be formally written as

$$d(\omega) \equiv \frac{1}{N} \text{Tr}(\delta(\mathcal{H}'_{\text{pair}} - \omega)) = \frac{1}{N} \sum_{j=0}^{N-1} \delta(\lambda_j - \omega), \tag{43}$$

where $N = 2^n = 2^6 = 64$ is the dimension of this Hilbert space, and λ_i is i -th eigenvalue of $\mathcal{H}'_{\text{pair}}$.

To approximate $d(\omega)$ computationally, one often replaces the Dirac- δ distribution by a smooth surrogate function such as a Gaussian or a Lorentzian [36]. If we use a Gaussian defined as $g(\omega) = \exp\left(-\frac{\omega^2}{2\sigma^2}\right)$ to replace the Dirac- δ distribution, $d(\omega)$ becomes

$$d(\omega) \approx \frac{1}{N} \text{Tr}(g(\mathcal{H}'_{\text{pair}} - \omega I)) = \frac{1}{N} \sum_{j=0}^{N-1} g(\lambda_j - \omega). \tag{44}$$

One way to develop a quantum algorithm to estimate $d(\omega)$ is to construct quantum circuits that can produce $|0^a\rangle |\psi_i\rangle + |0^a\rangle^\perp |\phi_i\rangle$, where $|\psi_i\rangle = \frac{1}{\sqrt{N}} \sum_{x=0}^{N-1} \sqrt{g(\mathcal{H} - \omega_i I)} |x\rangle |x\rangle$ for a set of sampled

energy levels ω_i , $i = 1, 2, \dots, m$ and a is the number of ancilla qubits, $|0^a\rangle^\perp$ denotes a quantum state orthogonal to $|0^a\rangle$ and $|\phi_i\rangle$ is a quantum state that we do not care about. Here $|x\rangle$ denotes an n -qubit computational basis where $n = \log N$. The success probability of measuring the ancilla qubits in the $|0\rangle^a$ state is $\langle\psi_i|\psi_i\rangle$, which is exactly $d(\omega_i)$ as

$$\begin{aligned}
\langle\psi_i|\psi_i\rangle &= \frac{1}{N} \sum_{x,y} [\sqrt{g(\mathcal{H}'_{\text{pair}} - \omega_i I)} |y\rangle |y\rangle]^\dagger \sqrt{g(\mathcal{H}'_{\text{pair}} - \omega_i I)} |x\rangle |x\rangle \\
&= \frac{1}{N} \sum_{x,y} \langle y | g(\mathcal{H}'_{\text{pair}} - \omega_i I) |x\rangle \langle y | x\rangle \\
&= \frac{1}{N} \sum_x \langle x | g(\mathcal{H}'_{\text{pair}} - \omega_i I) |x\rangle \\
&= \frac{1}{N} \text{Tr} [g(\mathcal{H}'_{\text{pair}} - \omega_i I)].
\end{aligned} \tag{45}$$

To produce $|0^a\rangle |\psi_i\rangle + |0^a\rangle^\perp |\phi_i\rangle$, we construct a circuit that block encodes $\sqrt{g(\mathcal{H}'_{\text{pair}} - \omega_i I)}$. This construction can be achieved by using QSP (Theorem 3.1) and QSVT. We label this circuit as U_{QSVT} in Figure 15 which presents the overall circuit structure used to produce $|0^a\rangle |\psi_i\rangle$ for a fixed ω_i .

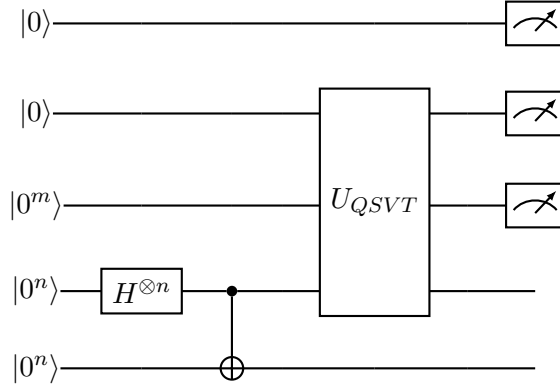


Figure 15: The overall structure of the circuit used to produce $|0\rangle^a |\psi_i\rangle$. The circuit block labelled by U_{QSVT} is the circuit that block encodes $\sqrt{g(\mathcal{H}'_{\text{pair}} - \omega_i I)}$. The superposition of all n -qubit computational basis $|\chi\rangle = \frac{1}{\sqrt{N}} \sum_x |x\rangle |x\rangle$ is prepared via the Hadamard gates and multi-qubit CNOT gate (Figure 16).

The general structure of the U_{QSVT} circuit is shown in Figure 17 where the circuit block labelled by U_B represents the block encoding circuit for $\mathcal{H}'_{\text{pair}}$, and the phase angle ϕ_j that appears in a single qubit gate $e^{-i\phi_j Z}$ can be obtained from the software package QSP-PACK [32, 37, 31]. These angles are computed by solving an optimization problem that minimizes the difference between $\sqrt{g(\lambda - \omega_j)}$ and a polynomial approximation $p(\lambda)$. The optimization problem can be simplified for even and odd functions. Therefore, to take advantage of this simplification, we modify the surrogate Gaussian function by replacing λ with $|\lambda|$ and obtain

$$\tilde{g}(\lambda - \omega_j) = \exp\left\{ \frac{(|\lambda| - \omega_j)^2}{2\sigma^2} \right\}.$$

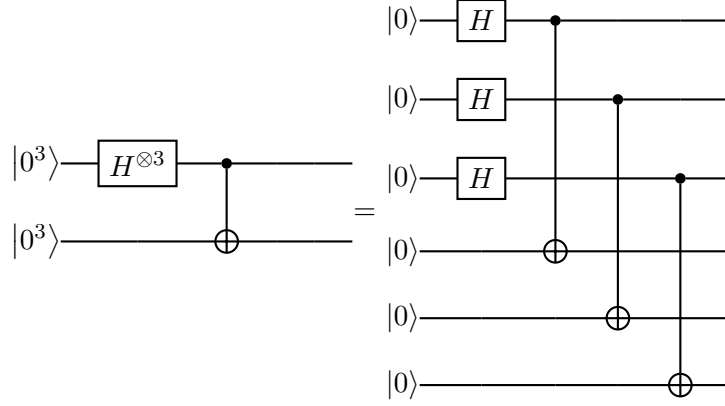


Figure 16: Illustration of the multi-qubit CNOT gate used to produce $|\chi\rangle$ in Figure 15 with $n = 3$.

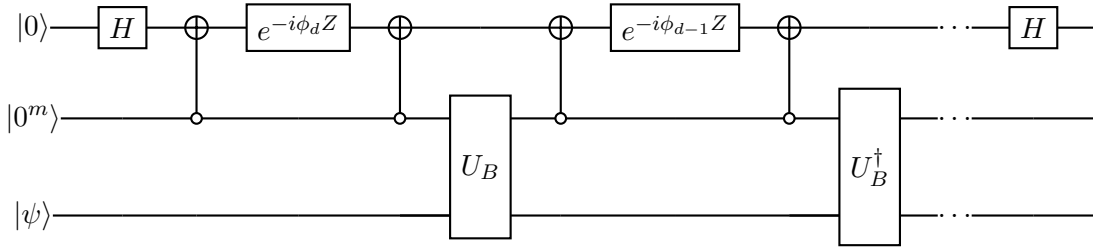


Figure 17: The circuit structure of the quantum singular value transformation. The phases are computed through QSP-PACK [32, 37, 31] for the function $\sqrt{\tilde{g}}(\lambda - \omega_j) = \exp\left\{\frac{(|\lambda - \omega_j|^2)}{4\sigma^2}\right\}$ with σ is set to be 0.01. When the QSP-PACK is used in the numerical experiments, we set the scaling factor to be 0.8, the maximum iteration of the optimization to be 200, and the precision to be 10^{-12} . We use the Newton method for the optimization and set two options *targetPre* and *useReal* in the QSP-PACK to be true and false, respectively.

The first two layers of the circuit shown in Figure 15 are used to prepare $|\chi\rangle = \frac{1}{\sqrt{N}} \sum_x |x\rangle |x\rangle$ needed to produce $|\psi_i\rangle = \frac{1}{\sqrt{N}} \sum_{x=0}^{N-1} \sqrt{g(\mathcal{H}'_{\text{pair}} - \omega_i I)} |x\rangle |x\rangle$. In this part of the circuit, we first apply n Hadamard gates to the first set of n qubits initialized as $|0\rangle$ to obtain the state $\frac{1}{\sqrt{N}} \sum_x |x\rangle |0^n\rangle$. We then use a series of CNOT gates placed on matching qubits to bring the second set of n qubits to be in the superposition of $|x\rangle$ also. Instead of measuring several ancilla qubits in Figure 15, additional CNOT gates can be used to reduce the number of ancilla qubits to be measured to 1. While the focus of this paper is on the circuit design for block encoding the second-quantized pairing Hamiltonian, we hold the discussions of the initial state preparation and measurement to future works.

Figure 18 shows the comparison between DOS obtained from the diagonalization of $\mathcal{H}'_{\text{pair}}$ and evaluating (44), which is shown as the solid curve, and the square amplitudes of ψ_i 's defined by (45) in which a polynomial of degree $d_{qsp} = 50$ is constructed (via QSP) to approximate $\sqrt{\tilde{g}(\lambda - \omega_i)}$, which are shown as solid square markers connected by a dotted curve. Because the circuit we construct produces a $(16, 5)$ -block encoding of $\mathcal{H}_{\text{pair}}$, the computed DOS is the DOS of $\mathcal{H}_{\text{pair}}/16$. We use the same \tilde{g} in both calculations. The former can be viewed as an exact DOS calculation and the latter can be interpreted as the DOS approximation obtained from the quantum algorithm presented in this section. This figure shows that the approximate DOS obtained from the quantum algorithm match well with exact DOS. All major peaks of the DOS can be correctly identified from the dotted curve within the spectrum interval of interest $[-0.05, 0.2]$.

As we indicated in section 4, the gate complexity for constructing a block encoding quantum circuit U_B for $\mathcal{H}'_{\text{pair}}$ is $\mathcal{O}(\text{poly}(n))$. The number of U_B blocks and the number of additional CNOT and phase gates in the QSVT circuit shown in Figure 17 depends on the degree of the polynomial required to accurately approximate $\tilde{g}(\omega)$, which in turn depends on the spectrum width and the required resolution of the DOS. With the degree of polynomial d_{qsp} in QSP being $\mathcal{O}(\text{poly}(n))$, the overall gate complexity for the quantum circuit associated with each ω_i is $\mathcal{O}(\text{poly}(n))$.

The query complexity of the quantum DOS approximation depends on the number of energy samples ω_i 's required to construct the DOS approximation and the number of measurements necessary for sufficient success measurements. If both scale as $\mathcal{O}(\text{poly}(n))$, then the overall complexity of the quantum DOS approximation is $\mathcal{O}(\text{poly}(n))$, which is superior to the $\mathcal{O}(\text{poly}(N))$ required in a classical DOS estimation algorithm [36]. However, for the restricted problem presented in this example, the total number of gates required in the circuit shown in Figure 15 exceeds $N = 64$ due to restricted problem size that is far from the asymptotic regime. A more detailed analysis of the quantum resources required to obtain a quantum DOS approximation is beyond the scope of this paper and will be addressed in future researches.

6 Conclusion

In this paper, we follow the general strategy presented in [1] to develop a direct and explicit way to construct a block encoding circuit for a nuclear pairing Hamiltonian by treating it as a sparse matrix with a special structure. The circuit consists of an O_C circuit block that encodes the sparsity structure of the Hamiltonian and an $O_{\mathcal{H}}$ circuit block that encodes the numerical values of the nonzero matrix elements in the Hamiltonian. The O_C block contains a sequence of controlled swap operations combined with controlled validation operations. The $O_{\mathcal{H}}$ block contains a sequence of controlled rotations. The gate complexity of the proposed block encoding circuit is $\mathcal{O}(\text{poly}(n))$ with n being the number of single-particle states used to represent the many-body wavefunctions associated with the Hamiltonian. The number of ancilla qubits required is $\log L + 3$

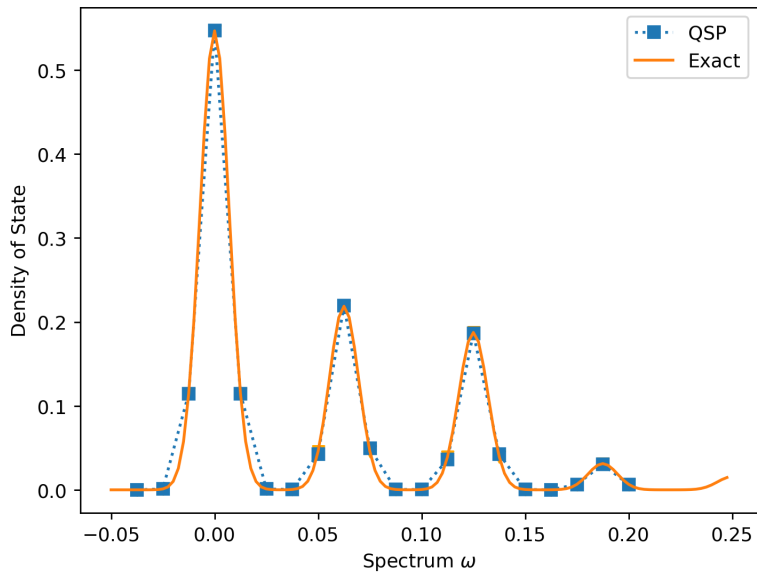


Figure 18: The density of states of the pairing Hamiltonian for all the possible many-nucleon systems supported by the restricted basis set. The solid line indicates the exact density of states via classical calculations. The squares connected by the dashed lines indicate the density of states from quantum computation. We employ $(d_{qsp} + 1)$ -th degree polynomial to approximate $\tilde{g}(\lambda - \omega_j)$. The QSP calculation is performed with $d_{qsp} = 50$ for good convergence.

where L is the number of terms in (13). In practice, L is typically a polynomial in n . Hence the number of ancilla qubits is $\mathcal{O}(\log(n))$. The gate complexity and ancilla qubit count are comparable to that required in a circuit that block encodes the pairing Hamiltonian after it is written as a linear combination of (unitary) Pauli operators (strings). We refer to this approach as the LCU block encoding scheme. We believe that being able to directly construct a block encoding circuit without resorting to mapping the creation and annihilation operators to the Pauli strings through the Jordan-Wigner (JW) or Bravyi-Kitaev (BK) transformations simplifies the circuit construction process and is more intuitive and clear. Utilizing the JW or BK transformation creates 16 Pauli strings for each two-body interaction term in the pairing Hamiltonian (13). One additional qubit is needed to account for the linear combination of these Pauli strings.

We have not performed a thorough analysis of the query complexity and success probability of measurement in the paper. However, we expect the success probability of measuring $|0\rangle$ from the output of the circuit presented here to be comparable to that associated with the block encoding circuit for the linear combination of Pauli strings since the l_1 norm of coefficients in both approaches are the same.

Although the O_C circuit block that consists of a sequence of controlled swap operations is comparable in structure to the select oracle used in the LCU based block encoding circuit, the $O_{\mathcal{H}}$ circuit block that contains a sequence of controlled rotations is considerably easier to construct in general than the prepare oracle circuit required in an LCU based approach. The prepare oracle in the LCU based approach requires encoding $8L$ coefficients that appear in the method presented in this paper. The advantage of constructing a circuit for $O_{\mathcal{H}}$ over a prepare oracle in LCU is also expected for a more general k -body Hamiltonian for $k > 2$.

We also note that, even though we have demonstrated a direct and explicit block encoding circuit construction for a second-quantized pairing Hamiltonian, the technique presented here is rather general and can be extended to any second-quantized many-body Hamiltonian. For a more general second-quantized Hamiltonian, the control used for the swap operation can potentially be more complex. However, there should not be any fundamental difficulties in implementing such a circuit block. The main issue that needs to be properly addressed is the presence of additional phase terms in the $c(j, l)$ function. These phase terms can be encoded by utilizing previously developed techniques that can be found in, for example, [17]. We also refer readers to works [19, 38] on addressing the phase terms in general second-quantized Hamiltonians of relativistic and nonrelativistic many-fermion systems.

Acknowledgments

This work was supported by US DOE Grant DE-SC0023707 under the Office of Nuclear Physics Quantum Horizons program for the "NuNuclei and Hadrons with Quantum computers (NuHaQ)" project (W.D., J.V.). This work was supported by Computing Sciences 2023 Summer Program at Berkeley Lab (D.L.). This work was also supported by the Quantum Systems Accelerator program (L.L., C.Y.), by the Applied Mathematics Program of the US Department of Energy (DOE) Office of Advanced Scientific Computing Research under contract number DE-AC02-05CH1123 (L.L.), the DOE Office of Advanced Scientific Computing Research Accelerated Research for Quantum Computing (ARQC) Program (C.Y.) under U.S. Department of Energy Contract No. DE-AC02-05CH11231. L.L. is a Simons Investigator in Mathematics.

References

- [1] Daan Camps, Lin Lin, Roel Van Beeumen, and Chao Yang. Explicit quantum circuits for block encodings of certain sparse matrices. *arXiv preprint arXiv:2203.10236*, 2022.
- [2] Guang Hao Low and Isaac L Chuang. Optimal hamiltonian simulation by quantum signal processing. *Physical review letters*, 118(1):010501, 2017.
- [3] Guang Hao Low and Isaac L Chuang. Hamiltonian simulation by qubitization. *Quantum*, 3:163, 2019.
- [4] András Gilyén, Yuan Su, Guang Hao Low, and Nathan Wiebe. Quantum singular value transformation and beyond: exponential improvements for quantum matrix arithmetics. In *Proceedings of the 51st Annual ACM SIGACT Symposium on Theory of Computing*, pages 193–204, 2019.
- [5] Michael A Nielsen and Isaac L Chuang. Quantum computation and quantum information. *Phys. Today*, 54(2):60, 2001.
- [6] Lin Lin. Lecture notes on quantum algorithms for scientific computation. *arXiv preprint arXiv:2201.08309*, 2022.
- [7] Andrew M Childs. Lecture notes on quantum algorithms. *Lecture notes at University of Maryland*, 2017.
- [8] Christoph Sünderhauf, Earl Campbell, and Joan Camps. Block-encoding structured matrices for data input in quantum computing. *arXiv preprint arXiv:2302.10949*, 2023.
- [9] Lin-Chun Wan, Chao-Hua Yu, Shi-Jie Pan, Su-Juan Qin, Fei Gao, and Qiao-Yan Wen. Block-encoding-based quantum algorithm for linear systems with displacement structures. *Phys. Rev. A*, 104:062414, Dec 2021.
- [10] Thomas Loke and Jingbo B Wang. Efficient quantum circuits for szegedy quantum walks. *Annals of Physics*, 382:64–84, 2017.
- [11] Daan Camps, Efehan Kökcü, Lindsay Bassman Oftelie, Wibe A De Jong, Alexander F Kemper, and Roel Van Beeumen. An algebraic quantum circuit compression algorithm for hamiltonian simulation. *SIAM Journal on Matrix Analysis and Applications*, 43(3):1084–1108, 2022.
- [12] Daan Camps and Roel Van Beeumen. Fable: Fast approximate quantum circuits for block-encodings. In *2022 IEEE International Conference on Quantum Computing and Engineering (QCE)*, pages 104–113. IEEE, 2022.
- [13] Daan Camps and Roel Van Beeumen. Approximate quantum circuit synthesis using block encodings. *Physical Review A*, 102(5):052411, 2020.
- [14] Jiaqi Leng, Joseph Li, Yuxiang Peng, and Xiaodi Wu. Expanding hardware-efficiently manipulable hilbert space via hamiltonian embedding. *arXiv preprint arXiv:2401.08550*, 2024.
- [15] SS Zhou and JB Wang. Efficient quantum circuits for dense circulant and circulant like operators. *Royal Society open science*, 4(5):160906, 2017.
- [16] Haoya Li, Hongkang Ni, and Lexing Ying. On efficient quantum block encoding of pseudo-differential operators. *Quantum*, 7:1031, 2023.

- [17] Kianna Wan. Exponentially faster implementations of select (h) for fermionic hamiltonians. *Quantum*, 5:380, 2021.
- [18] Ryan Babbush, Craig Gidney, Dominic W Berry, Nathan Wiebe, Jarrod McClean, Alexandru Paler, Austin Fowler, and Hartmut Neven. Encoding electronic spectra in quantum circuits with linear t complexity. *Physical Review X*, 8(4):041015, 2018.
- [19] Weijie Du and James P. Vary. Multinucleon structure and dynamics via quantum computing. *Phys. Rev. A*, 108(5):052614, 2023.
- [20] Ryan Babbush, Nathan Wiebe, Jarrod McClean, James McClain, Hartmut Neven, and Garnet Kin Chan. Low depth quantum simulation of electronic structure. *arXiv preprint arXiv:1706.00023*, 2017.
- [21] Ryan Babbush, Nathan Wiebe, Jarrod McClean, James McClain, Hartmut Neven, and Garnet Kin-Lic Chan. Low-depth quantum simulation of materials. *Physical Review X*, 8(1):011044, 2018.
- [22] Hans Hon Sang Chan, David Muñoz-Ramo, and Nathan Fitzpatrick. Simulating non-unitary dynamics using quantum signal processing with unitary block encoding. *arXiv preprint arXiv:2303.06161*, 2023.
- [23] Michael A Nielsen et al. The fermionic canonical commutation relations and the jordan-wigner transform. *School of Physical Sciences The University of Queensland*, 59, 2005.
- [24] Jacob T Seeley, Martin J Richard, and Peter J Love. The bravyi-kitaev transformation for quantum computation of electronic structure. *The Journal of chemical physics*, 137(22), 2012.
- [25] Andrew Tranter, Peter J Love, Florian Mintert, and Peter V Coveney. A comparison of the bravyi–kitaev and jordan–wigner transformations for the quantum simulation of quantum chemistry. *Journal of chemical theory and computation*, 14(11):5617–5630, 2018.
- [26] Maria Paola Lombardo Morten Hjorth-Jensen and Ubirajara van Kolck. *An Advanced Course in Computational Nuclear Physics: Bridging the Scales from Quarks to Neutron Stars (Lecture Notes in Physics, 936)*. Springer, 2017. 1st ed.
- [27] Jouni Suhonen. *From Nucleons to Nucleus: Concepts of Microscopic Nuclear Theory*. Springer, 2010. 1st ed.
- [28] John M. Martyn, Zane M. Rossi, Andrew K. Tan, and Isaac L. Chuang. Grand unification of quantum algorithms. *PRX Quantum*, 2:040203, Dec 2021.
- [29] M.A. Nielsen and I.L. Chuang. *Quantum Computation and Quantum Information: 10th Anniversary Edition*. Cambridge University Press, 2010.
- [30] Alastair Kay. Tutorial on the quantikz package. *arXiv preprint arXiv:1809.03842*, 2018.
- [31] Yulong Dong, Lin Lin, Hongkang Ni, and Jiasu Wang. Infinite quantum signal processing. *arXiv preprint arXiv:2209.10162*, 2022.
- [32] Yulong Dong, Xiang Meng, K. Birgitta Whaley, and Lin Lin. Efficient phase-factor evaluation in quantum signal processing. *Phys. Rev. A*, 103:042419, Apr 2021.

- [33] Rafaella Vale, Thiago Melo D Azevedo, Ismael Araújo, Israel F Araujo, and Adenilton J da Silva. Decomposition of multi-controlled special unitary single-qubit gates. *arXiv preprint arXiv:2302.06377*, 2023.
- [34] Vivek V Shende and Igor L Markov. On the cnot-cost of toffoli gates. *arXiv preprint arXiv:0803.2316*, 2008.
- [35] Weijie Du and James P. Vary. Multinucleon structure and dynamics via quantum computing. *Phys. Rev. A*, 108(5):052614, 2023.
- [36] Lin Lin, Yousef Saad, and Chao Yang. Approximating spectral densities of large matrices. *SIAM review*, 58(1):34–65, 2016.
- [37] Jiasu Wang, Yulong Dong, and Lin Lin. On the energy landscape of symmetric quantum signal processing. *Quantum*, 6:850, November 2022.
- [38] Weijie Du and James P Vary. Hamiltonian input model and spectroscopy on quantum computers. *arXiv preprint arXiv:2402.08969*, 2024.